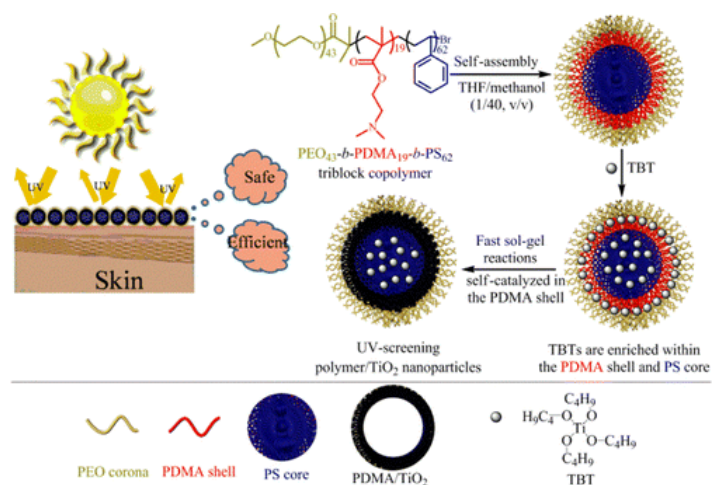


- Polymer/TiO<sub>2</sub> Hybrid Nanoparticles with Highly Effective UV-Screening but Eliminated Photocatalytic Activity

Xiao, J.; Chen, W.; Wang, F.; Du, J. *Macromolecules*, **2013**, *46*, 375-383.

Abstract:



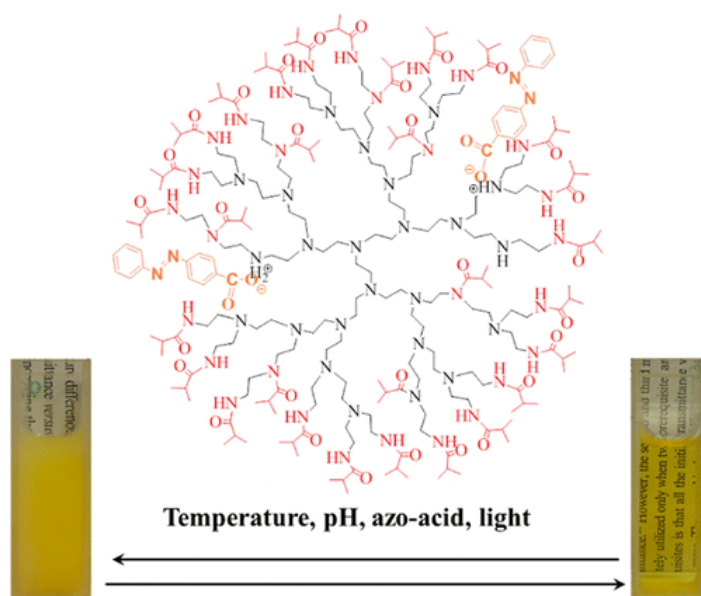
TiO<sub>2</sub> nanoparticle has been considered as a safe sunscreen agent to reduce the skin cancer risk when exposed to sunlight. However, recently it was found that TiO<sub>2</sub> particles accelerate the photodamage of skin due to their photocatalytic degradation activity. To effectively eradicate this unwanted effect, we present a new strategy toward the preparation of organic/inorganic hybrid polymer/TiO<sub>2</sub> nanoparticles with highly effective UV-screening property but eliminated photocatalytic activity. We prepared new polymer micelles with corona-shell-core structure based on self-assembly of poly(ethylene oxide)-block-poly(2-(dimethylamino)ethyl methacrylate)-block-poly(styrene) (PEO-b-PDMA-b-PS) triblock copolymer. Selective deposition of hydrophobic tetrabutyl titanate (TBT) in the PDMA shell in polar solvent leads to a thin PDMA/TiO<sub>2</sub> hybrid layer (~8 nm), which can not only effectively reflect UV rays but also eliminate its photocatalytic ability to protect skin. The sol-gel reactions of TBTs in the PS core domain lead to a PS/TiO<sub>2</sub> hybrid core, which can also absorb/reflect UV lights by PS/TiO<sub>2</sub>. The biocompatible PEO coronas can prevent direct contact of TiO<sub>2</sub> with skin. Moreover, sol-gel reactions in the PDMA and PS domains can stabilize the triblock copolymer micelles, which offer the promising potential for further formulations in aqueous solution. The ATRP kinetics confirmed that PEO-b-PDMA-b-PS triblock copolymer can be synthesized in one pot, which simplified the synthetic procedure of copolymers. TEM and DLS studies revealed the morphology and size of self-assembled polymer micelles and the subsequent polymer/TiO<sub>2</sub> hybrid nanoparticles upon sol-gel reactions. UV experiments confirmed the highly efficient UV screening activity but eliminated photocatalytic property of polymer/TiO<sub>2</sub> hybrid nanoparticles. For example, at extremely low TiO<sub>2</sub> content in solution (10 ppm of polymer/TiO<sub>2</sub> solid), ~70% UV radiation can be blocked compared to pure organic polymer micelle, which is also much more efficient than commercially available TiO<sub>2</sub> nanoparticles (P25). UV and DLS studies confirmed the ultrahigh stability of polymer/TiO<sub>2</sub> hybrid nanoparticles upon strong UV radiation, which is suitable for long-term applications. Nitrogen adsorption/desorption experiment revealed that the ultralow surface area of TiO<sub>2</sub> nanoparticles (1.6 m<sup>2</sup> g<sup>-1</sup>) is consistent with their extremely poor photocatalytic performance.

- Thermo-, pH-, and Light-Responsive Supramolecular Complexes Based on a Thermoresponsive Hyperbranched Polymer

Zhang, J.; Liu, H.-J.; Yuan, Y.; Jiang, S.; Yao, Y.; Chen, Y. *ACS Macro Lett.*, **2013**, *2*, 67-71.

Abstract:

2

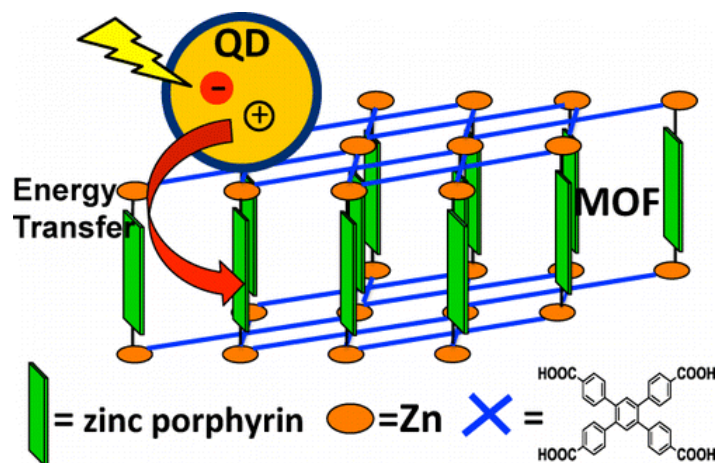


Hyperbranched polyethylenimine terminated with isobutyramide groups (HPEI-IBAm) was mixed with 4-(phenylazo)benzoic acid (PABA) to form supramolecular complexes through the neutralization reaction between the amino groups of HPEI-IBAm and the carboxylic acid group of PABA, which was verified by  $^1\text{H}$  and 2D NOESY  $^1\text{H}$  NMR spectroscopy. The obtained supramolecular complexes with a molar ratio of PABA to HPEI-IBAm of  $\leq 8$  were soluble in water and exhibited thermoresponsive properties. Their cloud point temperature ( $T_{\text{cp}}$ ) was sensitive to PABA content, and PABA molecules were exchanged between HPEI-IBAm hosts. The topology of the polymer affected the change in  $T_{\text{cp}}$  of the complexes. At pH  $\sim 7$ , increasing the PABA content decreased  $T_{\text{cp}}$ , whereas it caused  $T_{\text{cp}}$  to increase at pH  $\sim 9$ . Reversible trans-to-cis photoisomerization of azobenzene units in the complexes occurred following irradiation with UV or visible light. At pH  $\sim 7$ , trans-to-cis isomerization of azobenzene units increased  $T_{\text{cp}}$ , whereas the opposite occurred at pH  $\sim 9$ .

- Energy Transfer from Quantum Dots to Metal–Organic Frameworks for Enhanced Light Harvesting

Jin, S.; Son, H. J.; Farha, O. K.; Wiederrecht, G. P.; Hupp, J. T. *J. Am. Chem. Soc.* **2013**, *135*, 955–958.

Abstract:

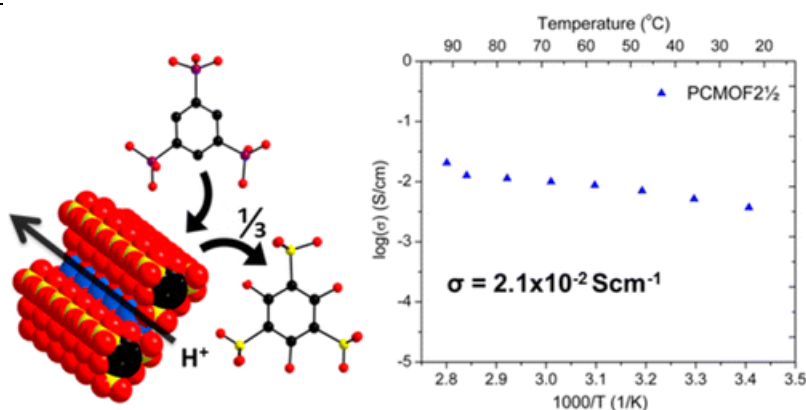


Because of their efficient energy-transport properties, porphyrin-based metal–organic frameworks (MOFs) are attractive compounds for solar photochemistry applications. However, their absorption bands provide limited coverage in the visible spectral range for light-harvesting applications. We report here the functionalization of porphyrin-based MOFs with CdSe/ZnS core/shell quantum dots (QDs) for the enhancement of light harvesting via energy transfer from the QDs to the MOFs. The broad absorption band of the QDs in the visible region offers greater coverage of the solar spectrum by QD–MOF hybrid structures. We show through time-resolved emission studies that photoexcitation of the QDs is followed by energy transfer to the MOFs with efficiencies of more than 80%. This sensitization approach can result in a >50% increase in the number of photons harvested by a single monolayer MOF structure with a monolayer of QDs on the surface of the MOF.

- Enhancing Proton Conduction in a Metal–Organic Framework by Isomorphous Ligand Replacement

Kim, S.; Dawson, K. W.; Gelfand, B. S.; Taylor, J. M.; Shimizu, G. K. H. *J. Am. Chem. Soc.* **2013**, *135*, 963–966.

Abstract:

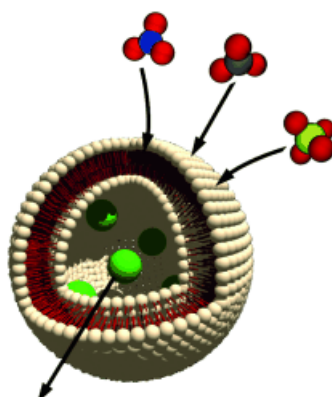


Using the concept of isomorphous replacement applied to entire ligands, a  $C_3$ -symmetric trisulfonate ligand was substituted with a  $C_3$ -symmetric tris(hydrogen phosphonate) ligand in a proton conducting metal–organic framework (MOF). The resulting material, PCMOF2<sup>1/2</sup>, has its proton conduction raised 1.5 orders of magnitude compared to the parent material, to  $2.1 \times 10^{-2} \text{ S cm}^{-1}$  at 90% relative humidity and 85 °C, while maintaining the parent MOF structure.

- Small-Molecule Lipid-Bilayer Anion Transporters for Biological Applications

Busschaert, N.; Gale, P. A. *Angew. Chem. Int. Ed.* **2013**, *52*, 1374–1382.

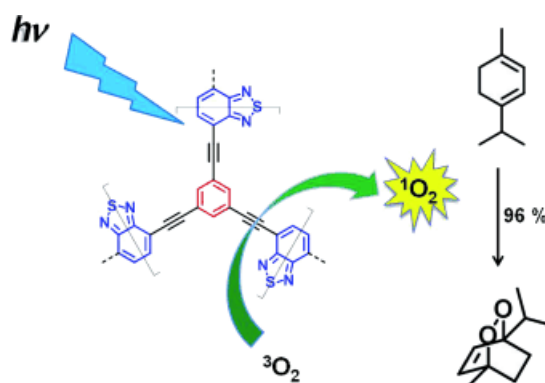
Abstract:



**Into the cell:** The development of small-molecule lipid-bilayer anion transporters for potential future use in channel replacement therapy for the treatment of cystic fibrosis, and in treating cancer by perturbing chemical gradients within cells, is currently an area of intense interest. This Minireview looks at recent developments in the design of small-molecule transmembrane anion transporters and focuses on the progress so far in employing these compounds in biological systems.

- Surface Area Control and Photocatalytic Activity of Conjugated Microporous Poly(benzothiadiazole) Networks  
Zhang, K.; Kopetzki, D.; Seeberger, P. H.; Antonietti, M.; Vilela, F. *Angew. Chem. Int. Ed.* **2013**, *52*, 1432–1436.

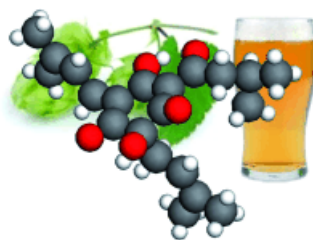
Abstract:



Conjugated microporous polymers (CMPs) with controlled specific surface area have been prepared through Sonogashira–Hagihara cross-coupling reactions in the presence of silica nanoparticles as templating agents. The CMPs act as heterogeneous photosensitizers for producing singlet oxygen in a continuous flow synthesis (see picture).

- Absolute Configuration of Beer’s Bitter Compounds  
Urban, J.; Dahlberg, C. J.; Caroll, B. J.; Kaminsky, W. *Angew. Chem. Int. Ed.* **2013**, *52*, 1553–1555.

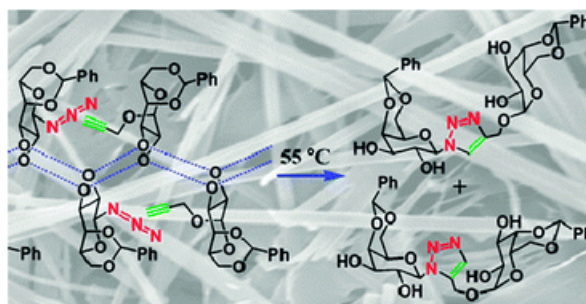
Abstract:



**During the beer brewing process**, bitter tasting *cis* and *trans* iso- $\alpha$ -acids are generated from the precursor  $\alpha$ -acids found in hops. The absolute configurations of the  $\alpha$ -acid (–)-humulone and several of its derivatives have now been elucidated by X-ray crystallography, thus resolving decades of confusion over the humulone isomerization mechanism.

- Supramolecular design of a bicomponent topochemical reaction between two non-identical molecules  
Krishnan, B. P.; Ramakrishnan, S.; Sureshan, K. M. *Chem. Commun.* **2013**, *49*, 1494–1496

Abstract:

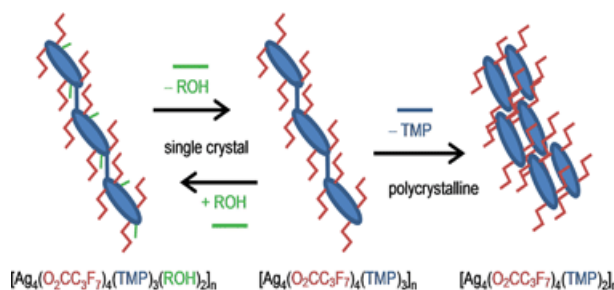


We report the first design of a topochemical reaction between two non-identical reactants using a supramolecular chemistry approach. A coassembly of two sugar-based organogelators with complementary reacting motifs, viz. azides and alkynes, undergoes topochemical Huisgen reaction between them.

- Chemical transformations of a crystalline coordination polymer: a multi-stage solid–vapour reaction manifold

Vitórica-Yrezábal, I. J.; Espallargas, G. M.; Soleimannejad, J.; Florence, A. J.; Fletcher, A. J.; Brammer, L. *Chem. Sci.* **2013**, *4*, 696–708.

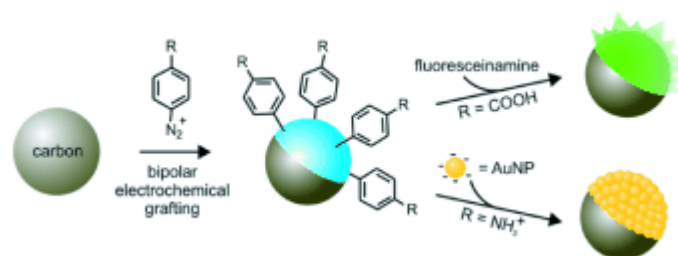
Abstract:



In its crystal structure the one-dimensional coordination polymer  $[\text{Ag}_4(\text{O}_2\text{C}(\text{CF}_2)_2\text{CF}_3)_4(\text{TMP})_3]_n$  (**1**) (TMP = 2,3,5,6-tetramethylpyrazine) adopts a zig-zag arrangement in which pairs of silver(I) centres bridged by two fluorocarboxylate ligands are linked alternately *via* one or two neutral TMP ligands. This material can reversibly absorb/desorb small alcohols (ROH) in single-crystal-to-single-crystal transformations, despite the lack of porosity in the crystals, to yield a related material of formula  $[\text{Ag}_4(\text{O}_2\text{C}(\text{CF}_2)_2\text{CF}_3)_4(\text{TMP})_3(\text{ROH})_2]_n$  (**1-ROH**). The absorption process includes coordination of the alcohol to silver(I) centres and, in the process, insertion of the alcohol into one-quarter of the Ag–O bonds of coordination polymer. When in place, the alcohol molecule is also supported by formation of an O–H  $\cdots$  O hydrogen bond to the now partially dissociated carboxylate group. The reverse process leading to desorption of the alcohol takes place upon mild heating to regenerate **1**. Upon further heating, **1** can release molecules of TMP into the vapour phase resulting in a *separate* chemical and structural transformation to yield a two-dimensional layered material of composition  $[\text{Ag}_4(\text{O}_2\text{C}(\text{CF}_2)_2\text{CF}_3)_4(\text{TMP})_2]_n$  (**2**). This new transformation occurs *via* dissociation of Ag–N bonds upon ligand release and formation of new Ag–O bonds. The whole series of transformations has been followed *in situ* by single-crystal and/or powder X-ray diffraction and studied by thermogravimetric analysis. As a mechanistic probe to explore transport within formally nonporous **1**, gravimetric CO<sub>2</sub> gas sorption/desorption has been conducted. It is proposed that transport of small molecules occurs through the fluororous layers in the crystal.

- Wireless Electrografting of Molecular Layers for Janus Particle Synthesis  
Kumsapaya, C.; Bakai, M.-F.; Loget, G.; Goudeau, B.; Warakulwit, C.; Limtrakul, J.; Kuhn, A.; Zigah, D. *Chem. Eur. J.* **2013**, *19*, 1577-1580.

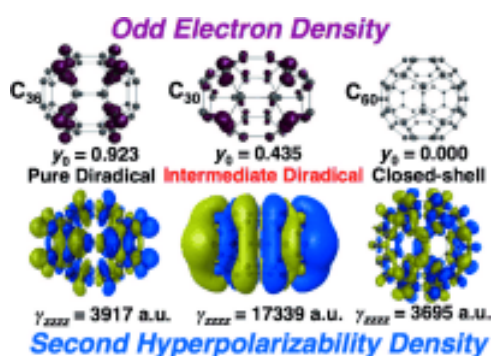
Abstract:



**Glassy carbon beads** are selectively functionalized on one side with an ultrathin organic layer by bipolar electrochemical reduction of diazonium salts to give Janus-type beads with a hybrid organic–inorganic composition (see scheme). The presence of the grafted organic layers is revealed either by co-adsorption of gold nanoparticles or by coupling with a fluorescent molecule.

- Interplay between the Diradical Character and Third-Order Nonlinear Optical Properties in Fullerene Systems  
Muhammad, S.; Fukuda, K.; Minami, T.; Kishi, R.; Shigeta, Y.; Nakano, M. *Chem. Eur. J.* **2013**, *19*, 1677-1685.

Abstract:



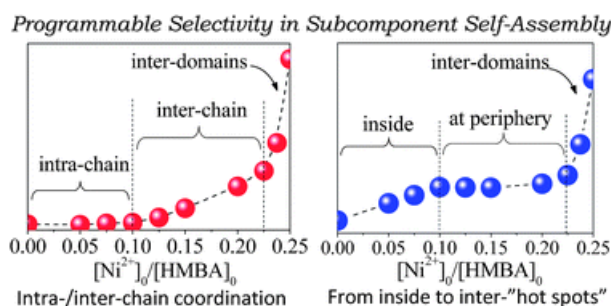
To reveal new structure–property relationships in the nonlinear optical (NLO) properties of fullerenes that are associated with their open-shell character, we investigated the interplay between the diradical character ( $y_i$ ) and second hyperpolarizability (longitudinal component,  $\gamma_{zzzz}$ ) in several fullerenes, including  $C_{20}$ ,  $C_{26}$ ,  $C_{30}$ ,  $C_{36}$ ,  $C_{40}$ ,  $C_{42}$ ,  $C_{48}$ ,  $C_{60}$ , and  $C_{70}$ , by using the broken-symmetry density functional theory (DFT; LC-UBLYP ( $\mu=0.33$ )/6-31G\*//UB3LYP/6-31G\*). We found that the large differences between the geometry and topology of fullerenes have a significant effect on the diradical character of each fullerene. On the basis of their different diradical character, these fullerenes were categorized into three groups, that is, closed-shell ( $y_i=0$ ), intermediate open-shell ( $0 < y_i < 1$ ), and almost pure open-shell compounds ( $y_i \approx 1$ ), which originated from their diverse topological features, as explained by odd-electron-density and spin-density diagrams. For example, we found that closed-shell fullerenes include  $C_{20}$ ,  $C_{60}$ , and  $C_{70}$ , whereas fullerenes  $C_{26}$  and  $C_{36}$  and  $C_{30}$ ,  $C_{40}$ ,  $C_{42}$ , and  $C_{48}$  are pure and intermediate open-shell compounds, respectively. Interestingly, the  $\gamma_{zzzz}$  enhancement ratios between  $C_{30}/C_{36}$  and  $C_{40}/C_{60}$  are 4.42 and 11.75, respectively, regardless of the smaller  $\pi$ -conjugation size in  $C_{30}$  and  $C_{40}$  than in  $C_{36}$  and  $C_{60}$ . Larger  $\gamma_{zzzz}$  values were obtained for other fullerenes that had intermediate diradical character, in accordance with our previous valence configuration interaction (VCI) results for the two-site diradical model. The  $\gamma_{zzzz}$  density analysis shows that the large positive

contributions originate from the large  $\gamma_{zzzz}$  density distributions on the right- and left-extended edges of the fullerenes, between which significant spin polarizations (related to their intermediate diradical character) appear within the spin-unrestricted DFT level of theory.

- Programmable selectivity of metal-imine bond coordination in subcomponent self-assembly of a primary amine based block copolymer

Chen, X.; Xu, N.; Li, N.; Lu, L.; Cai, Y.; Zhao, Y.; Wang, D. *Soft Matter* **2013**, *9*, 1885-1894.

Abstract:

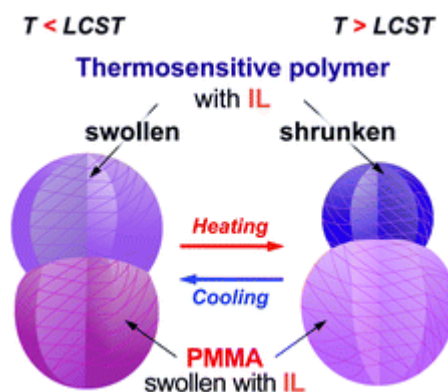


We describe the programmable selectivity of intra-/inter-chain coordination in the subcomponent self-assembly of a primary amine based block copolymer. A well-defined poly(6-amino-hexylmethacrylamide hydrochloride)-*block*-poly(*N*-2-hydroxypropylmethacrylamide) (PHPMA-*b*-PAHMA) was synthesized *via* visible light activated aqueous RAFT polymerisation at 25 °C. The conjugation of 2-hydroxy-5-methoxybenzaldehyde (HMBA) in the absence or presence of small fractions of the nickel ion complex was monitored using  $^1\text{H}$  NMR and UV spectroscopy. Subcomponent self-assembly and the programmable selectivity of intra-/inter-chain coordination were studied using dynamic light scattering and  $^1\text{H}$  NMR. The results demonstrated that the coordinated HMBA was much more reactive than the free HMBA, which promoted the collapse and hydrophobic association of polymer chains and thus brought about the autocatalysis of imine formation inside the collapsed "hot spots". The polymer chains progressively assembled into narrowly-distributed nanoparticles on adding small fractions of  $\text{Ni}^{\text{II}}(\text{HMBA})_2$  rather than autopoietically splitting into smaller ones, as observed on adding pure HMBA. More importantly, the diversity of subcomponent self-assembly and solubility of aggregates originated from the programmable selectivity of intra-/inter-chain coordination.

- Preparation of free-standing thermosensitive composite gel particles incorporating ionic liquids

Suzuki, T.; Ichikawa, H.; Nakai, M.; Minami, H. *Soft Matter* **2013**, *9*, 1761-1765.

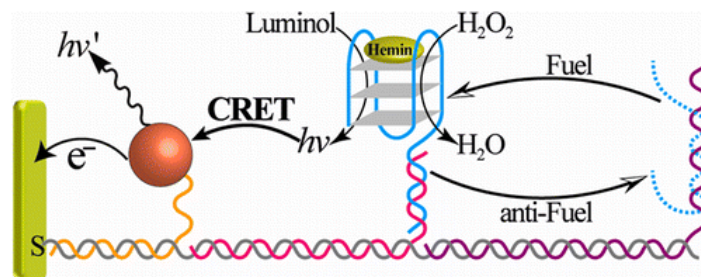
Abstract:



Composite gel particles consisting of 2-phenylethyl methacrylate (PhEMA)-vinyl toluene (VT) copolymer (P(PhEMA-VT)) and poly(methyl methacrylate) (PMMA) were prepared by seeded polymerization of MMA in the presence of P(PhEMA-VT)/1-butyl-3-methylimidazolium bis(trifluoromethanesulfonyl)amide ([Bmim][TfSA], IL) gel particles, in which P(PhEMA-VT) exhibited lower critical solution temperature (LCST)-type phase transition behavior in IL. The particles obtained at 70 °C (above the LCST) adopted a phase-separated snowman-like shape and clearly exhibited volume–phase transition behavior in which the P(PhEMA-VT) phase reduced in size and the PMMA phase increased in size above the LCST. The P(PhEMA-VT) phase exhibited LCST-type volume–phase transition behavior and separation of IL occurred. In contrast, the PMMA phase was swollen with IL separated from the P(PhEMA-VT) phase, in which the PMMA phase could act as a preserver of IL. Interestingly, the composite gel particles exhibited similar volume–phase transition behavior in both air and vacuum without leakage of IL from the gel particles, which should be free-standing thermosensitive gel particles.

- Switching Photonic and Electrochemical Functions of a DNAzyme by DNA Machines  
Liu, X.; Niazov-Elkan, A.; Wang, F.; Willner, I. *Nano Lett.* **2012**, i, 219-225.

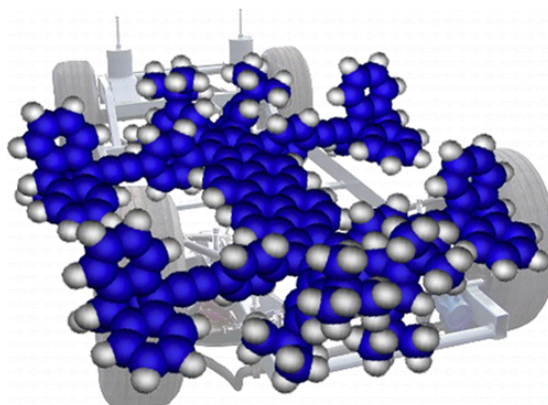
Abstract:



DNA nanostructures acting as DNA machines are described. Specifically, DNA “walkers” assembled on nucleic acid scaffolds and triggered by fuel/antifuel strands are activated in solution or on surfaces, for example, electrodes or semiconductor CdSe/ZnS quantum dots (QDs). The DNA machines led to the switchable formation or dissociation of the hemin/G-quadruplex DNAzyme on the DNA scaffolds. This enabled the chemiluminescence, chemiluminescence resonance energy transfer (CRET), electrochemical, or photoelectrochemical transduction of the switchable states of the different DNA machines.

- Molecule Concept Nanocars: Chassis, Wheels, and Motors?  
Joachim, C.; Rapenne, G. *ACS Nano* **2013**, 7, 11-14.

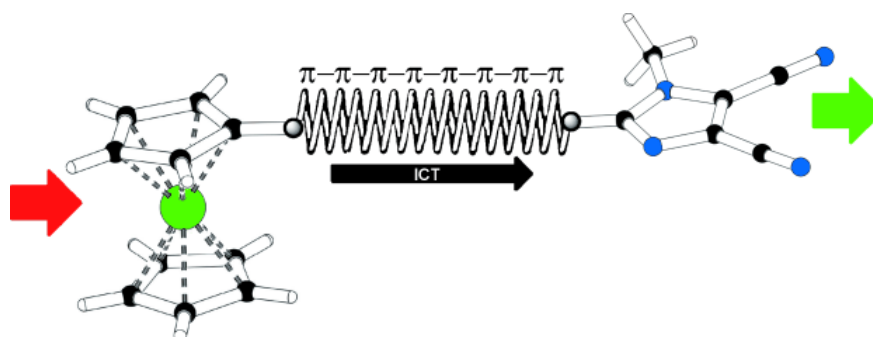
Abstract:



The design, synthesis, and running of a molecular nanovehicle on a surface assisted by proper nanocommunication channels for feeding and guiding the vehicle now constitute an active field of research and are no longer a nano-joke. In this Perspective, we describe how this field began, its growth, and problems to be solved. Better molecular wheels, a molecular motor with its own gears assembling for torque transmission must be mounted on (i.e., chemically bonded to) a good molecular chassis for the resulting covalently constructed molecular nanovehicle to run on a surface in a controlled manner at the atomic scale. We propose a yearly molecule concept nanocar contest to boost molecular nanovehicle research.

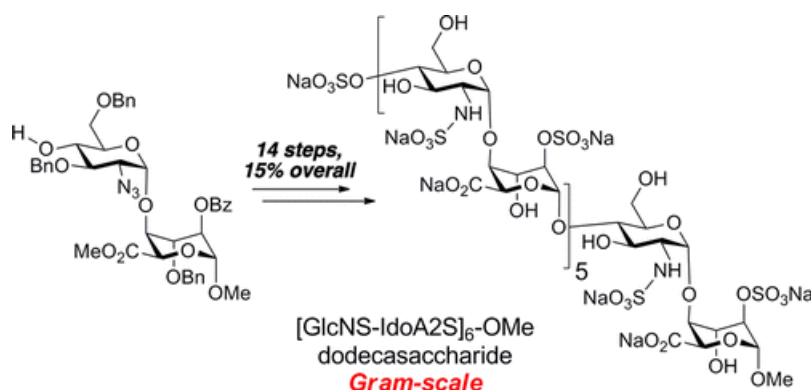
- Ferrocene-Donor and 4,5-Dicyanoimidazole-Acceptor Moieties in Charge-Transfer Chromophores with  $\pi$  Linkers Tailored for Second-Order Nonlinear Optics  
Kulhánek, J.; Bureš, F.; Kuznik, W.; Kityk, I.V.; Mikysek, T.; Růžička, A. *Chem. Asian. J.* **2013**, *8*, 465-475.

Abstract:



A series of new nonlinear optical chromophores (**1–15**) that were comprised of ferrocene-donor and 4,5-dicyanoimidazole-acceptor moieties and various  $\pi$  linkers of different length were synthesized. Support for the presence of significant D—A interactions in these NLO-phores was obtained from the evaluation of the quinoid character of the 1,4-phenylene moieties and their electronic absorption spectra, which featured intense high-energy (HE) bands that were accompanied by less-intense low-energy (LE) bands. The redox behavior of these compounds was investigated by cyclic voltammetry (CV) and by rotating-disc voltammetry (RDV); their electrochemical gaps decreased steadily from 2.64 to 2.09V. In addition to the experimentally obtained data, DFT calculations of their absorption spectra, HOMO/LUMO levels, and second-order polarizabilities ( $\beta$ ) ( $-2\omega, \omega, \omega$ ) were performed. A structure–property relationship study that was performed by systematically altering the  $\pi$  linker revealed that the intramolecular charge-transfer and nonlinear optical properties of these inorganic–organic hybrid D— $\pi$ —A systems (**1–15**) were primarily affected by: 1) The presence of olefinic/acetylenic subunits; 2) the length of the  $\pi$  linker; and 3) the spatial arrangement (planarity) of the  $\pi$  linker.

- First Gram-Scale Synthesis of a Heparin-Related Dodecasaccharide  
Hansen, S.U.; Miller, G. J.; Jayson, G. C., Gardiner, J.M. *Org. Lett.* **2013**, *15*, 88-91.  
Abstract:

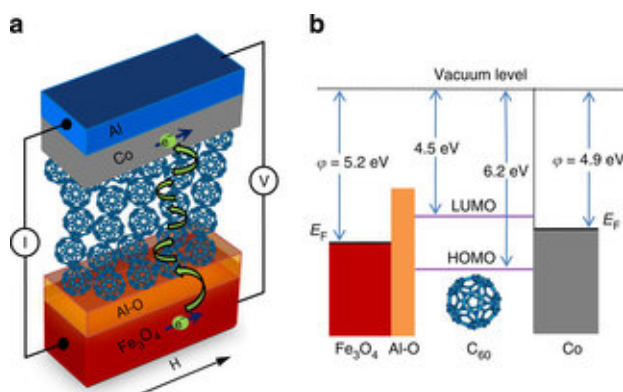


The first example of a gram-scale synthesis of a structurally defined, heparin-related dodecasaccharide is reported. An iterative 14-step process using an iduronate donor disaccharide delivers >1g quantities of the dodecasaccharide sequence [GlcNS-IdoA2S]<sub>6</sub>-OMe in 15% overall yield from the reducing terminal disaccharide, a 2 orders of magnitude increase in scale for access to synthetic heparanoid dodecasaccharide mimetics. The synthesis also delivers multigram amounts of the protected oligosaccharides from tetra- through to dodecasaccharide.

- Observation of a large spin-dependent transport length in organic spin valves at room temperature

Zhang, X.; Mizukami, S.; Kubota, T.; Ma, Q.; Oogane, M.; Naganuma, H.; Ando, Y.; Miyazaki, T. *Nature Communications* **2013**, *4*, 1392.

Abstract:

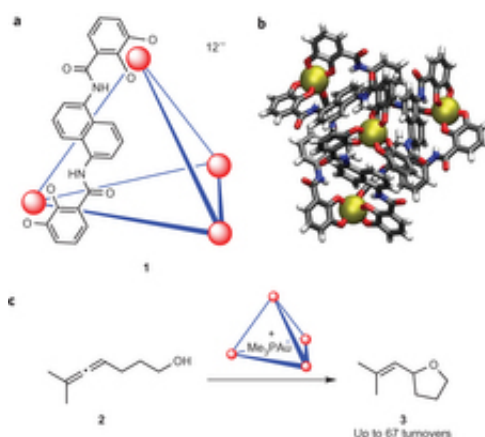


The integration of organic semiconductors and magnetism has been a fascinating topic for fundamental scientific research and future applications in electronics, because organic semiconductors are expected to possess a large spin-dependent transport length based on weak spin-orbit coupling and weak hyperfine interaction. However, to date, this length has typically been limited to several nanometres at room temperature, and a large length has only been observed at low temperatures. Here we report on a novel organic spin valve device using C<sub>60</sub> as the spacer layer. A magnetoresistance ratio of over 5% was observed at room temperature, which is one of the highest magnetoresistance ratios ever reported. Most importantly, a large spin-dependent transport length of approximately 110 nm was experimentally observed for the C<sub>60</sub> layer at room temperature. These results provide insights for further understanding spin transport in organic semiconductors and may strongly advance the development of spin-based organic devices.

- A supramolecular approach to combining enzymatic and transition metal catalysis  
Wang, Z. J.; Clary, K. N.; Bergman, R. G.; Raymond, K. N.; Toste, F. D. *Nature Chemistry*

2013, 5, 100–103.

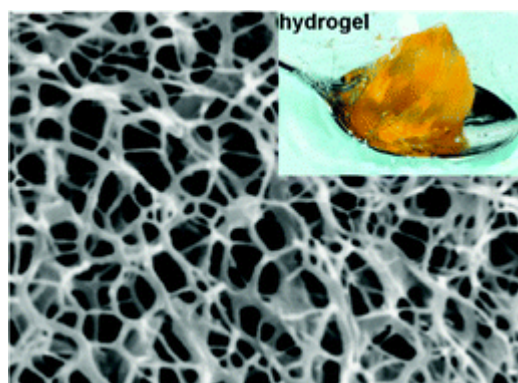
Abstract:



The ability of supramolecular host–guest complexes to catalyse organic reactions collaboratively with an enzyme is an important goal in the research and discovery of synthetic enzyme mimics. Herein we present a variety of catalytic tandem reactions that employ esterases, lipases or alcohol dehydrogenases and gold(I) or ruthenium(II) complexes encapsulated in a  $\text{Ga}_4\text{L}_6$  tetrahedral supramolecular cluster. The host–guest complexes are tolerated well by the enzymes and, in the case of the gold(I) host–guest complex, show improved reactivity relative to the free cationic guest. We propose that supramolecular encapsulation of organometallic complexes prevents their diffusion into the bulk solution, where they can bind amino-acid residues on the proteins and potentially compromise their activity. Our observations underline the advantages of the supramolecular approach and suggest that encapsulation of reactive complexes may provide a general strategy for carrying out classic organic reactions in the presence of biocatalysts.

- Recombinant proteins as cross-linkers for hydrogelations  
Wang, H.; Shi, Y.; Wang, L.; Yang, Z. *Chem. Soc. Rev.* **2013**, *42*, 891-901.

Abstract:

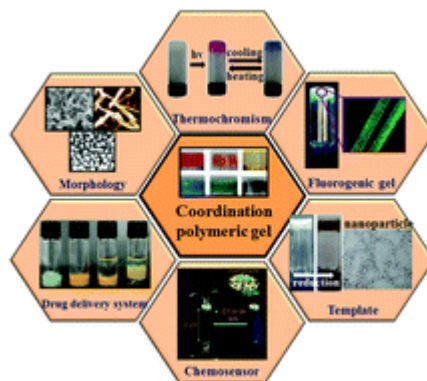


Protein-based hydrogels are promising materials for tissue engineering and drug delivery due to the unique properties of proteins such as perfect polydispersity, exact control over monomer sequence, ability to fine-tune molecular-level biochemical interactions, *etc.* This tutorial review summarizes recent progress on the preparation of protein-based hydrogels and their applications. Typically, we introduce two strategies of covalent and non-covalent ones for the preparation of hydrogels. Hydrogels prepared by the covalent strategy are stable and can respond to the conformational change of proteins. They can be applied for cells encapsulation, screening of drug molecules and heavy metals, *etc.* Hydrogels formed by non-covalent interactions are injectable physical hydrogels.

The simple mixing preparation strategy and fast gelation kinetics guarantee the homogeneous encapsulation of cells and therapeutic agents within them. Therefore, they have been widely applied for the delivery of bioactive components, regenerative medicine, *etc.* The challenges that remained in this field are also summarized in this paper. We envision that rationally designed protein-based hydrogels will have broad applications in many areas including controlled delivery, tissue engineering, drug screening, *etc.*

- Coordination polymer gels with important environmental and biological applications  
Jung, J. H.; Lee, J. H.; Silverman, J. R.; John, G. *Chem. Soc. Rev.* **2013**, *42*, 924-936.

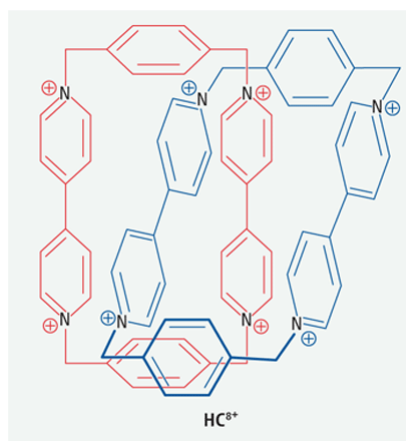
Abstract:



Coordination Polymer Gels (CPGs) constitute a subset of solid-like metal ion and bridging organic ligand structures (similar to metal–organic frameworks) that form multi-dimensional networks through a trapped solvent as a result of non-covalent interactions. While physical properties of these gels are similar to conventional high molecular weight organic polymer gels, coordination polymer gel systems are often fully reversible and can be assembled and disassembled in the presence of additional energy (heat, sonication, shaking) to give a solution of solvated gelators. Compared to gels resulting from purely organic self-assembled low molecular weight gelators, metal ions incorporated into the fibrillar networks spanning the bulk solvent can impart CPGs with added functionalities. The solid/liquid nature of the gels allows for species to migrate through the gel system and interact with metals, ligands, and the solvent. Chemosensing, catalysis, fluorescence, and drug-delivery applications are some of the many potential uses for these dynamic systems, taking advantage of the metal ion's coordination, the organic polydentate ligand's orientation and functionality, or a combination of these properties. By fine tuning these systems through metal ion and ligand selection and by directing self-assembly with external stimuli the rational synthesis of practical systems can be envisaged.

- Corraling Positively Charged Molecular Radicals  
Benniston, A. *Science* **2013**, *339*, 404-405.

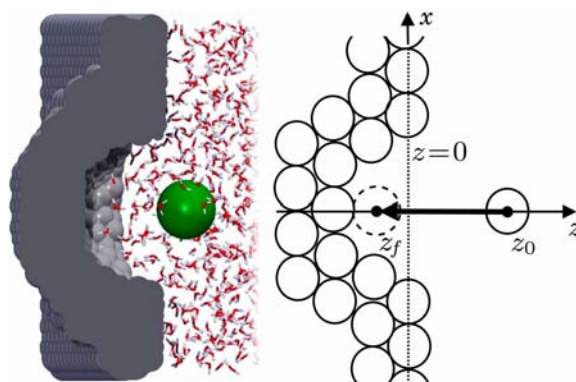
Abstract:



At the outset, the idea of forcing together multiple positive charges onto an organic molecule and ending up with a stable interlocked supramolecular structure seems destined for failure. Coulombic repulsion forces usually extract an energetic penalty on adding an additional charge onto a highly charged molecule, and the organic radicals that would form with stepwise charge addition are likely to be unstable. On page 429 of this issue, Barnes *et al.* (1) show that counterintuitive thinking about this problem can reap rewards. They show that a [2]catenane molecule, in which two identical rings interlock noncovalently like links of a chain (2), displays a rich vein of electrochemical responses. This homocatenane (HC) can stabilize organic radicals and bear up to eight positive charges.

- Solvent fluctuations in hydrophobic cavity–ligand binding kinetics  
Piotr Setny, P.; Baron, R.; Kekenes-Huskey, P. M.; McCammon, J. A.; Dzubiella, J. *Proc. Natl. Acad. Sci. USA* **2013**, *110*, 1197-1202.

Abstract:



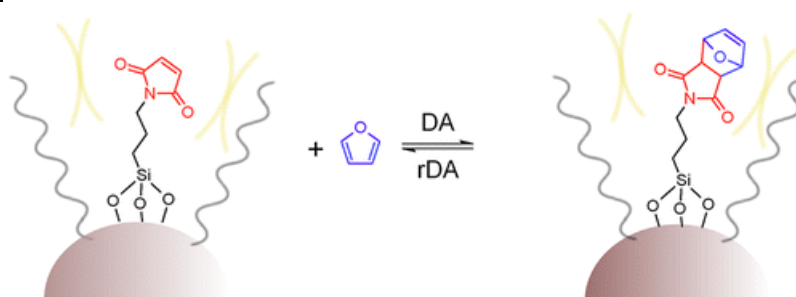
Water plays a crucial part in virtually all protein–ligand binding processes in and out of equilibrium. Here, we investigate the role of water in the binding kinetics of a ligand to a prototypical hydrophobic pocket by explicit-water molecular dynamics (MD) simulations and implicit diffusional approaches. The concave pocket in the unbound state exhibits wet/dry hydration oscillations whose magnitude and time scale are significantly amplified by the approaching ligand. In turn, the ligand's stochastic motion intimately couples to the slow hydration fluctuations, leading to a sixfold-enhanced friction in the vicinity of the pocket entrance. The increased friction considerably decelerates association in the otherwise barrierless system, indicating the importance of molecular-scale hydrodynamic effects in cavity–ligand binding arising due to capillary fluctuations. We derive and analyze the diffusivity profile and show that the mean first passage time distribution from the MD simulation can be accurately reproduced by a standard Brownian dynamics simulation if the appropriate position-dependent friction profile is included. However, long-time decays in the water–ligand (random) force

autocorrelation demonstrate violation of the Markovian assumption, challenging standard diffusive approaches for rate prediction. Remarkably, the static friction profile derived from the force correlations strongly resembles the profile derived on the Markovian assumption apart from a simple shift in space, which can be rationalized by a time–space retardation in the ligand’s downhill dynamics toward the pocket. The observed spatiotemporal hydrodynamic coupling may be of biological importance providing the time needed for conformational receptor–ligand adjustments, typical of the induced-fit paradigm.

- Thermoreversible Reactions on Inorganic Nanoparticle Surfaces: Diels–Alder Reactions on Sterically Crowded Surfaces

Engel, T.; Kickelbick, G. *Chem. Mater.* **2013**, *25*, 149-157.

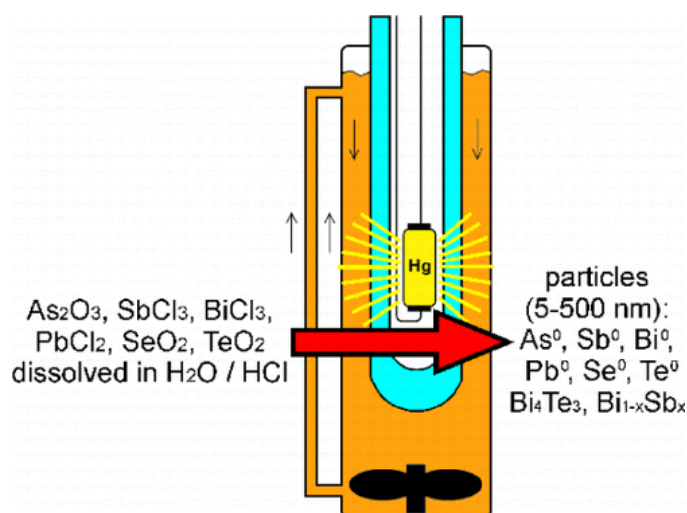
Abstract:



Organically surface-functionalized nanoparticles are important cross-linkers for nanocomposites. In the past, many cross-linking reactions were based on simple radical additions. However, novel smart materials require reversible reactions. These reactions, such as the Diels–Alder reaction, often have a specific sterical demand, e.g., a six-centered transition state. In this study, < 5 nm silica particles were functionalized with maleimide groups, and their reactivity with regard to Diels–Alder reactions were investigated, applying various techniques. A new method for the surface modification of silica nanoparticles is presented, minimizing agglomeration in organic solvents and thus increasing the accessibility of the functional groups on the particle surface. Kinetic studies of substituted model compounds were carried out to evaluate the reactivity of the maleimide functionality. The Diels–Alder reaction between 2,5-dimethylfuran and N-propylmaleimide, N-ethyl(N-propylcarbamato)maleimide, and N-phenylmaleimide was followed by UV/Vis spectroscopy. The reaction rate increases in this order, showing the effect of maleimide substitution. Afterwards N-((3-triethoxysilyl)propyl)maleimide was used to graft maleimidopropyl functional groups onto the nanoparticle surface. 3-Aminopropyltriethoxysilane, which could then be reacted with 1,1'-(methylenedi-4,1-phenylene)bismaleimide, was used to attach phenyl-substituted maleimide functionality to the surface. 3-Isocyanatopropyltriethoxysilane introduced the electron-drawing carbamato functionality into the system. The surface coverage of the samples was characterized applying CHN analysis, TGA-FTIR coupling, and FTIR spectroscopy. All analytical methods revealed that the functional groups are covalently bonded to the silica surface and the maleimide rings remain intact. Diels–Alder reactions of the surface groups show that the reactivity of the molecules attached to the particles depends on sterical crowding, but the reaction rate is not significantly changed by surface effects.

- Photochemical Synthesis of Particulate Main-Group Elements and Compounds  
Luz, A.; Malek-Luz, A.; Feldmann, C. *Chem. Mater.* **2013**, *25*, 202-209.

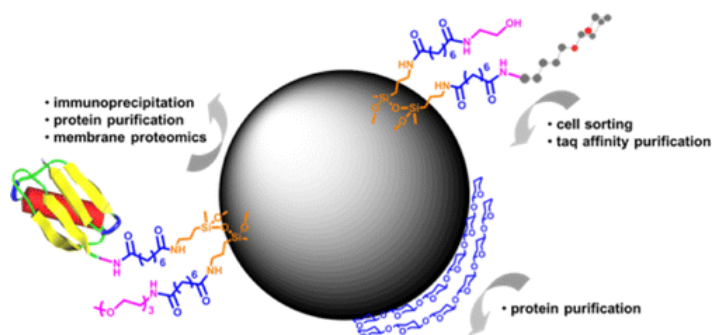
Abstract:



Particulate main-group elements ( $\text{As}^0$ ,  $\text{Sb}^0$ ,  $\text{Bi}^0$ ,  $\text{Pb}^0$ ,  $\text{Se}^0$ ,  $\text{Te}^0$ ) and compounds ( $\text{Bi}_4\text{Te}_3$ ,  $\text{Sb}_x\text{Bi}_{1-x}$  with  $0 \leq x \leq 1$ ) are obtained via photoinitiated reduction under UV irradiation. The synthesis of  $\text{Bi}^0$  and  $\text{Se}^0$  is exemplarily studied in detail. Here, meso- to micrometer-scaled particles are obtained with mean diameters of 81(11) nm ( $\text{Bi}^0$ ) and 1.15(18)  $\mu\text{m}$  ( $\text{Se}^0$ ) in the absence of specific stabilizers that allow controlling the particle growth. In contrast, the particle diameter is significantly reduced in the presence of specific stabilizers (e.g., polyvinylpyrrolidone/PVP for  $\text{Bi}^0$ , 2-mercaptoacetid acid/MAA for  $\text{Se}^0$ ). Now, even the nanoregime is reached with mean diameters of 4(2) nm ( $\text{Bi}^0$ ) and 290(39) nm ( $\text{Se}^0$ ). The photochemical synthesis is easy to perform (i.e., aqueous solution/suspension, room temperature, conventional chlorides/oxides as starting materials) and leads to a homogeneous particle nucleation, only initiated by UV irradiation as an external physical trigger. The resulting particulate main group elements and compounds are characterized by electron microscopy (SEM), dynamic light scattering (DLS), X-ray powder diffraction (XRD), and energy-dispersive X-ray (EDX) analysis. The mechanism of the light-initiated reaction can be clarified by polymerization experiments to involve radicals as intermediate species.

- A Chemically Functionalized Magnetic Nanoplatform for Rapid and Specific Biomolecular Recognition and Separation  
Lin, P.-C.; Yu, C.-C.; Wu, H.-T.; Lu, Y.-W.; Han, C.-L.; Su, A.-K.; Chen, Y.-J.; Lin, C.-C. *Biomacromolecules* **2013**, *14*, 160–168.

Abstract:



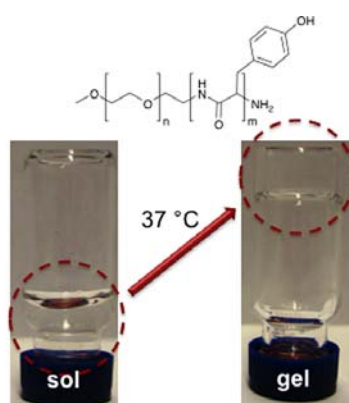
We have developed a target-molecule-functionalized magnetic nanoparticle (MNP)-based method to facilitate the study of biomolecular recognition and separation. The superparamagnetic property of MNPs allows the corresponding biomolecules to be rapidly separated from crude biofluids with a significant improvement in recovery yield and specificity. Various MNPs functionalized with tag

molecules (chitin, heparin, and amylose) were synthesized for recombinant protein purification, and several probe-functionalized MNPs, such as nitrilotriacetic acid (NTA)@MNP and Pk@MNP, exhibited excellent extraction efficiency for proteins. In a cell recognition study, mannose-functionalized MNPs allowed specific purification of *Escherichia coli* with FimH adhesin on the surface. In an immunoprecipitation assay, the antibody-conjugated MNPs reduced the incubation time from 12 to 1 h while maintaining a comparable efficiency. The functionalized MNPs were also used in a membrane proteomic study that utilized the interaction between streptavidin-functionalized MNPs and biotinylated cell membrane proteins. Overall, the functionalized MNPs were demonstrated to be promising probes for the specific separation of targets from proteins to cells and proteomics.

- Supramolecular Hydrogels with Reverse Thermal Gelation Properties from (Oligo)tyrosine Containing Block Copolymers

Huang, J.; Hastings, C. L.; Duffy, G. P.; Kelly, H. M.; Raeburn, J.; Adams, D. J.; Heise, A. *Biomacromolecules* **2013**, *14*, 200–206.

Abstract:

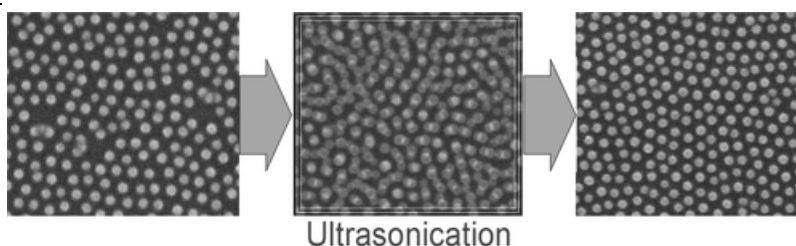


Novel block copolymers comprising poly(ethylene glycol) (PEG) and an oligo(tyrosine) block were synthesized in different compositions by N-carboxyanhydride (NCA) polymerization. It was shown that PEG2000-Tyr6 undergoes thermoresponsive hydrogelation at a low concentration range of 0.25–3.0 wt % within a temperature range of 25–50°C. Cryogenic transmission electron microscopy (Cryo-TEM) revealed a continuous network of fibers throughout the hydrogel sample, even at concentrations as low as 0.25 wt %. Circular dichroism (CD) results suggest that better packing of the  $\beta$ -sheet tyrosine block at increasing temperature induces the reverse thermogelation. A preliminary assessment of the potential of the hydrogel for *in vitro* application confirmed the hydrogel is not cytotoxic, is biodegradable, and produced a sustained release of a small-molecule drug.

- Increasing the Order Parameter of Quasi-Hexagonal Micellar Nanostructures by Ultrasound Annealing

Williges, C.; Chen, W.; Morhard, C.; Spatz, J. P.; Brunner, R. *Langmuir* **2013**, *29*, 989–993.

Abstract:



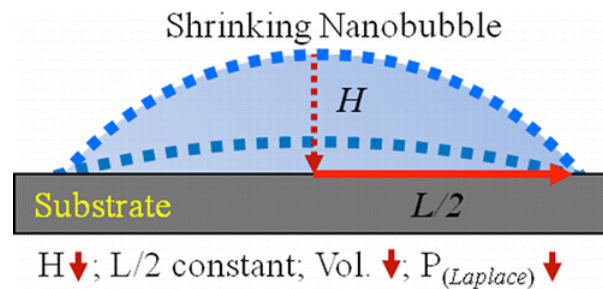
Nanopatterning with block copolymers finds many applications ranging from optics to bioscience. Many of these uses demand highly ordered patterns that are difficult to obtain because of environmental influences during fabrication. Here we demonstrate that ultrasonication improves the hexagonal order of artificially disturbed micellar nanopatterns.

17

- Stability of Interfacial Nanobubbles

Zhang, X.; Chan, D. Y. C.; Wang, D.; Maeda N. *Langmuir* **2013**, *29*, 1017–1023.

Abstract:

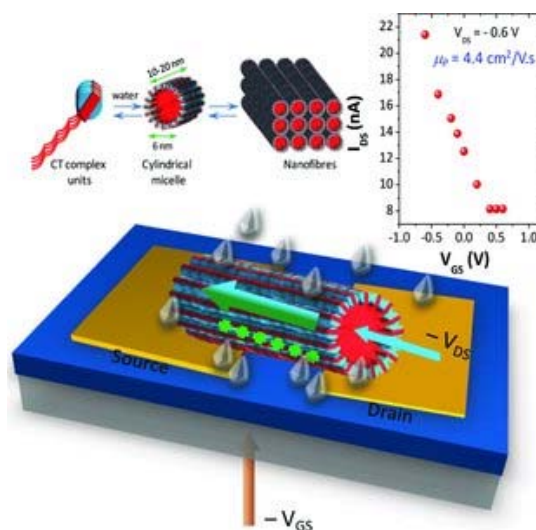


Interfacial nanobubbles (INBs) on a solid surface in contact with water have drawn widespread research interest. Although several theoretical models have been proposed to explain their apparent long lifetimes, the underlying mechanism still remains in dispute. In this work, the morphological evolution of INBs was examined in air-equilibrated and partially degassed water with the use of atomic force microscopy (AFM). Our results show that (1) INBs shrank in the partially degassed water while they grew slightly in the air-equilibrated water, (2) the three-phase boundary of the INBs was pinned during the morphological evolution of the INBs. Our analyses show that (1) the lifetime of INBs was sensitive to the saturation level of dissolved gases in the surrounding water, especially when the concentration of dissolved gases was close to saturation, and (2) the pinning of the three-phase boundary could significantly slow down the kinetics of both the growth and the shrinkage of the INBs. We developed a one-dimensional version of the Epstein–Plesset model of gas diffusion to account for the effect of pinning.

- High-Mobility Field Effect Transistors Based on Supramolecular Charge Transfer Nanofibres

Sagade, A. A.; Rao, K. V.; Mogera, U.; George, S. J.; Datta, A.; Kulkarni, G. U. *Adv. Mater.* **2013**, *25*, 559–564.

Abstract:



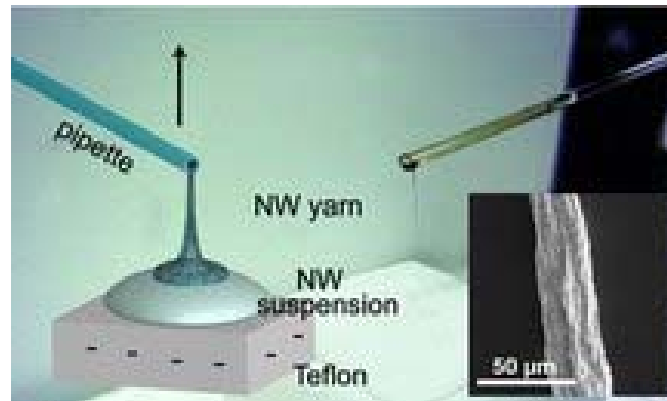
**Self-assembled charge transfer supramolecular nanofibres of coronene tetracarboxylate (CS)** and dodecyl substituted unsymmetrical tricyanogen derivative (DMV) behave as active channel in field effect transistors exhibiting high mobility. These devices work in ambient conditions and can regenerate in the presence of a single drop of water.

18

- Light Induced Nanowire Assembly: The Electrostatic Alignment of Semiconductor Nanowires into Functional Macroscopic Yarns

Petchsang, N.; McDonald, M. P.; Sinks, L.E.; Kuno, M. *Adv. Mater.* **2013**, *25*, 601–605.

Abstract:



**The electrostatic alignment and directed assembly of semiconductor nanowires into macroscopic, centimeter-long yarns** is demonstrated. Different morphologies can be produced, including longitudinally segmented/graded yarns or mixed composition fibers. Nanowire yarns display long range photoconductivities and open up exciting opportunities for potential use in future nanowire-based textiles or in solar photovoltaics.